Performance of Mn-based H_2S sorbents in dry, reducing atmosphere – support effects

Svatopluk Chytil[a,*], Milly Kure[b], Rune Lødeng[a] and Edd A. Blekkan[b]

[a] SINTEF Materials and Chemistry, Department of Kinetic and Catalysis, Postbox 4760, Sluppen, N-7465 Trondheim, Norway

[b] Department of Chemical Engineering, Norwegian University of Science and Technology (NTNU), N-7491 Trondheim, Norway

* Corresponding author. Tel.: +47 982 68 159

E-mail address: svatopluk.chytil@gmail.com (Svatopluk Chytil)

Abstract:

High temperature H_2S sorbents comprising manganese oxide (15 wt. %) supported on TiO_2, ZrO_2, CeO_2 and Al_2O_3 were prepared by wet impregnation using $Mn(NO_3)_2.4H_2O$ as Mn precursor. Upon activation in H_2, the sorbent performance testing was conducted at 650 °C in a model gas mixture with a composition of 0.4 vol. % of H_2S in 40 vol. % of H_2, the balance being inert gas (N_2 and Ar). Sorbent regeneration was performed at 650 °C with 5.2 vol. % of O_2 in N_2. The initial sorption performance is first reported for the parent (Mn-free) supports showing a considerable H_2S sorption on ZrO_2 and CeO_2 and a minor sorption on Al_2O_3 and TiO_2. The Mn sorbents were subject to 13 sorption/regeneration cycles. The highest initial sorption capacity is reported for cerium supported Mn oxide, which is also the sample that deactivates most. A prolonged exposure to H_2 at 650 °C results in a reversible loss of the sorption capacity that was observed for all the samples except for Mn on zirconia suggesting its superior stability in H_2.

The supports, fresh and regenerated Mn sorbents were characterized by means of N_2 sorption measurements, X-Ray Diffraction and Raman spectroscopy. Temperature-Programmed Reduction was performed on the parent supports and fresh sorbents. The changes in material properties caused by the testing as well as a different degree of a metal oxide-support interaction influencing the sorption performance are discussed.

Keywords:

Producer gas, H_2S solid sorbents, manganese oxides, support effect

Highlights:

- Additive effect observed for cerium supported manganese oxide due to H_2S sorption on the support as well as on the Mn oxide
- Superior stability of zirconium supported Mn oxide in H_2
- Strong metal oxide-support interaction influences the sorbent performance

Introduction

The product gas from gasification termed as a producer gas contains besides the main components (H_2, CO, CO_2, CH_4, C_2's, N_2, H_2O) some impurities such as dust, tar, NH_3, H_2S, COS, HCl and some trace elements (e.g. alkaline and alkaline metal earth metals and other inorganics) [1, 2, 3]. If the use of the producer gas requires advanced materials such as catalysts or fuel cells, the impurities need to be removed or reduced down to a very low level .For some applications as low concentrations as 60 ppb have been reported to be necessary [4]. In the case that the gas is to be used in the Solid Oxide Fuel Cell technology or in the Fischer-Tropsch synthesis utilizing Co based catalyst, the required H_2S limits typically are reported to be 1 ppm [5, 6].

Achieving such low concentrations is possible by solvent based absorption methods. However, the processes may lower the thermal efficiency due to cooling and subsequent reheating of the gas and the investment cost is often too high [7 - 9]. The use of solid sorbents has become increasingly important in biomass based process where the capacity of the plant is fairly small.

Mn oxides are together with Zn- and Fe-based sorbents often studied as suitable candidates for the H_2S removal from the producer gas. However, the high temperature can induce a formation of carbides and metallic Zn for the Fe and Zn oxides respectively [7, 8]. This may suppress the sorbent capacity and even cause some problems in the downstream processing. It has also been reported that the H_2S sorption kinetics, which is one of the key parameters when choosing a suitable sorbent, is more favorable for the Mn oxides when compared to the Zn ones [10].

An important aspect when selecting a sorbent is its durability and stability under the reaction conditions. In a recent work, performed with a model producer gas and using Mn_xO_y-Al_2O_3 sorbents, some performance decay over multiple sorption/regeneration cycles was observed [11]. As it was suggested that the use of alumina may be partly responsible for the deactivation, the use of other supports for the Mn oxide was examined. In this contribution we first present H_2S sorption data obtained for the parent supports in order to clarify whether the supports themselves are capable of

removing H_2S from the model gas mixture under the experimental conditions used. The sorption performance for Mn oxides supported on CeO_2, ZrO_2 and TiO_2 are then compared to the performance of Mn_xO_y-Al_2O_3 and also considering the performance of the parent support.

Characterization by means of fundamental methods is also presented here which allows evaluating the material properties relevant for the sorption as well as the change of the properties upon the multiple sorption/regeneration cycles. A particular attention is also devoted to the interaction between the support material and Mn as it is reasonable to expect that it may influence the sorbent performance.

Experimental

Chemicals

All chemicals and gases were used as received without further purification. The γ – alumina support LOT# B5160010 and purity 96 % was obtained from Strem chemicals. $Mn(NO_3)_2.4H_2O$ purum p.a. and Titanium (IV) oxide *puriss* was purchased from Sigma Aldrich. Zirconium oxide LOT#J10T008 was received from Alfa Aesar. Cerium (III) nitrate hexahydrate, 99.99 % metal basis was purchased from Sigma Aldrich.

Sample preparation

As-received alumina was calcined in an oven under static air conditions at 500 °C for 10 h prior to its functionalization with Mn. The CeO_2 support was obtained by the heating of the cerium nitrate precursor in an oven under air static conditions at 600 °C for 10 h [12]. As-received TiO_2 was also treated in air under static conditions at 700 °C for 10 h prior to its impregnation with the Mn salt in aqueous solution [13].

The manganese sorbents were prepared by the wet impregnation method using the Mn nitrate precursor, the parent supports and deionized water. Following the impregnation, the samples were dried at 100 °C for 24 h. Calcination of the samples was performed at 600 °C in static air for a period of 5 h. The heating rate used was 1 °C/ min. The nominal Mn loading was 15 wt. %. The sorbent samples are assigned with a prefix Mn15 followed by the support name used; e.g. Mn15-Al_2O_3. The regenerated samples after the multiple sorption/regeneration cycles are denoted with an affix –R; e.g. Mn15- Al_2O_3-R.

Instrumentation

Nitrogen adsorption-desorption isotherms were measured using a Micromeritics TriStar 3000 instrument. Prior to the measurement, the samples were outgassed at 100 °C for 12 hours. The specific surface area of the solids was evaluated by the BET method (Brunauer-Emmett-Teller) in the range of relative pressures p/p_0 = 0.1- 0.3. The pore size distributions were obtained from the adsorption branch of the isotherm using the Broekhoff – De Boer algorithms [14].

X-ray diffraction analysis (XRD) of the solid materials were performed on a Bruker AXS D8 Focus diffractometer using CuK_α radiation (λ=1.54 Å).

Raman spectroscopy measurements were performed on a Horiba Jobin Yvon, LABRAM HR 800 instrument. A laser excitation source of 633 nm was used and focused with a 50 × objective.

TPR measurements were performed on an in-house built apparatus [15]. Typically, the sample was heated in the temperature range 50 – 850 °C using a heating rate of 10 °C/min. For the CeO_2 and Mn15-CeO_2 sample, an extended temperature range 50 – 1000 °C was used. The reduction behavior of the samples was measured in a gas mixture consisting of 7 vol. % of H_2 in Ar.

The laboratory set-up used to measure the sorption-regeneration cycles consists of a gas feeding and metering system, a quartz fixed bed reactor and an analytical section. The set-up is described in detail elsewhere [11]. The gas concentrations are measured continuously by a ThermoStar GSD 320 T1 C analytical system equipped with a quadruple mass spectrometer QMS 200 using a secondary electron multiplier (SEM) or Faraday cup detector. The set-up was used without any significant modification. However, an additional thermocouple was installed on the external wall of the quartz rector in order to monitor the changes of the reactor temperature.

Prior to the sorption experiment, the sample was reduced in-situ in the H_2/N_2 mixture (50 ml/min) during the heating to the reaction temperature and then for approximately one hour before the sorption experiments. The system was then flushed with N_2. Consequently, the sorption gas was introduced first to the bypass and when the concentration of all the presented species was stable (as monitored by the MS), the sorption gas was directed to the reactor.

The feed gas composition for the sorption was 0.4, 39.6, 40.0 and 20 vol. % for H_2S, Ar, H_2 and N_2 respectively. A rather high H_2S concentration was used in order to facilitate a large number of sorption/regeneration cycles during the testing period. The sorbent regeneration was conducted in a gas mixture containing 5.2 vol. % of O_2 in N_2. The total gas flow used for the sorption and regeneration was 50 ml/min and the sample mass was 0.1 g. The concentration of the components present in the sorption gas was measured quantitatively as based on a regular calibration of the MS. However, the O_2 and SO_2 concentration during the regeneration was monitored only qualitatively following the *m/z* values of O_2 and SO_2. N_2 contained in the model gas mixture was used as an internal standard to calibrate the MS, while the second inert gas Ar diluted H_2S in the supplied gas mixture (1 vol. % H_2S in Ar).

The sorption and regeneration were performed at 650 °C and 101.325 kPa. The sorbent particle size was typically in the range 150 – 250 µm and it was not diluted with any additional solids. The length of the sorbent bed was approximately 4 mm and the reactor inner diameter was 6 mm. In total 13

sorption/regeneration cycles were performed for each sorbents sample while 1-2 cycles were performed on the parent supports. The parent supports were activated/ pretreated in the reducing atmosphere in the same manner as the Mn containing sorbents. For the Mn sorbents, the first and the thirteenth sorption cycle were run until complete sorbent saturation while the remaining sorption cycles were terminated when a H_2S concentration of 0.1 vol. % in the outlet was reached. In between each sorption/regeneration cycle the system was flushed with N_2. During the longer breaks between the cycles (overnight), the system was kept under N_2/H_2 flow at the reaction temperature. The total flow in that case was 20 ml/min and the composition was the same as used for the activation i.e. 50 vol. % of H_2 in N_2. Afterwards, an increased flow of 50 ml/min of the same gas mixture was used for approx. 1 h. The system was then flushed with N_2 and a new sorption cycle initiated. The cycles performed after the long exposures of the sample to the reducing environment are cycles numbered 2, 7, and 12.

Results and discussion

H_2S sorption on parent supports

The parent supports were activated in the H_2/N_2 mixture prior to the sorption measurements. The H_2S concentration profiles (H_2S in the exit gas as a function of time) measured over the solids at 650 °C and 101.325 kPa are depicted in Fig. 1. For the sake of the comparison, the figure also contains data measured in an empty reactor. Generally, the first part of the H_2S concentration profile measured represents the period when a stable flow of the sorption gas is established in the bypass. After this period, the sorption gas is directed to the rector, which is observed as a step change in the H_2S concentration. Then, depending on the sample ability to capture H_2S from the model gas, the low H_2S concentration is retained indicating that H_2S is efficiently removed by the material. The minimal H_2S concentrations measured in this period were typically in the range 0 – 100 ppm. This period provides a quantitative measure of the sample performance and can be used to estimate the sorbent

capacity. After this period the H_2S concentration returns back to its original value which is often assigned as the breakthrough. An irreversible, continuous rise of the H_2S concentration above approx. 100 ppm was used as the breakthrough point to calculate the sorbent capacity.

As seen in Fig. 1., the results obtained in the empty reactor suggest that there is no considerable H_2S adsorption in the reactor system as the H_2S concentration returns nearly instantly to its original value upon letting the gas into the reactor. This provides a good baseline for the measurements on the supports.

Results for the TiO_2 support show that there is only a slightly larger H_2S adsorption than the one observed in the empty reactor. From the experimental data it is impossible to distinguish to which extent the diffusion of H_2S through the solids bed might be responsible for this behavior. It can however be concluded that the H_2S adsorption on the reduced TiO_2 support under the experimental conditions is minimal.

Al_2O_3 shows a higher H_2S adsorption ability than TiO_2, but also in this case the capacity is rather low. On the other hand, the pre-reduced ZrO_2 shows a noticeable ability to adsorb H_2S from the model gas. The H_2S concentration profile recorded on the sample exhibits a typical sorption behavior as previously observed on the Mn_xO_y-Al_2O_3 sorbents under similar conditions [11]. The reduced cerium oxide also shows a considerable H_2S sorption capacity. However, in the latter case a significant "pre-breakthrough" sorption is observed. This is not an unusual sorption behavior as a similar sorption feature was observed by others for CeO_2 [16, 17]. Some authors attributed this phenomenon to the reaction of S that may remain in the set-up from the previous regeneration run with H_2 present in the model gas [17]. This may however not be the case in this study as the start-up procedures were identical for all the samples and the only sample that exhibits this behavior is the cerium oxide. Hence a series of additional experiments was performed with an aim to shed more light on this sorption characteristic. The experiment were conducted with two particle sizes in the range 50 – 150 µm in addition to the standard particle size used for the experiment (150 – 250 µm). The results

obtained on the finer fractions were however fairly identical to those presented in Fig. 1. It may therefore be suggested that a variation in the thickness of the sulfided layer (Ce_2O_2S) formed on the solid and the consequent H_2S diffusion through this layer probably is not responsible for the sorption characteristics observed on the CeO_2 sample, at least not with the particle sizes used in these experiments. There are possibly also some other reasons that may cause this behavior which will be discussed together with the characterization data. The overall sorption capacity of the supports tested decreases in the following order (1):

$CeO_2 > ZrO_2 > Al_2O_3 > TiO_2$

The fact that the metal oxides reacts with H_2S suggests that the materials shall not be regarded as "true" supports in this work. H_2S sorption on various unreduced metal oxides was in detail studied by Ziolek et al. [18, 19]. The mechanism of the H_2S interaction with the solids was discussed in the light of the acid/basic site strength which was coupled with the activity measurement of the sulfided and un-sulfided solids in several test reactions [18, 19]. However, the experimental conditions and the set-up to measure the H_2S sorption were quite different from the conditions used here. Therefore it is not attempted to make a direct comparison of the absolute sorption capacity values but rather focus on the overall trend. The reactivity patterns of the solids as represented in the sequence (1) are in line with the results presented by Ziolek et al. A considerable sorption takes place on the oxides having the highest number of basic sites (CeO_2 and ZrO_2), while the solids possessing a considerable Lewis acid site strength (TiO_2 and Al_2O_3) show rather low reactivity towards H_2S [19]. Interestingly, the results presented on the H_2-treated solids (Fig. 1) and unreduced materials [18] show an identical trend. For both ZrO_2 and CeO_2 it is expected that oxygen contained in the materials plays an important role as it is thought to be replaced by S_{ads}^{-II} upon the dissociative H_2S adsorption on ZrO_2 or directly exchanged by sulfur upon H_2S adsorption on CeO_2 [18,19]. As a considerable H_2S sorption is also observed on the reduced solids (Fig 1.), the susceptibility of the oxygen species for the interaction with sulfur persists and is not prevented by the reduction. For the CeO_2 material it

was shown that its sorption performance is improved after activation in H_2 as the reduced oxide was capable of more efficient removal of H_2S from the producer gas [17]. Also for a pre-reduced ZrO_2 it was shown that the material reacts with H_2S in an increasing amount in the tested temperature range 30 – 400 °C [20]. It was also deduced from the TPD and TPR experiments that the adsorbed S species are highly stable under reducing conditions in contrast to oxidizing conditions when their removal will likely take place via SO_x formation [20].

H_2S sorption on supported manganese oxide sorbents

Experimental data obtained on the reduced Mn based sorbents together with the data measured on ZrO_2 and CeO_2, are shown in Fig. 2. The results were collected in the same manner as the results for the parent supports except that the former data are collected over a larger number of sorption/regeneration cycles. As shown in Fig. 2, the sorption characteristic are quite alike for the Mn15-Al_2O_3 and Mn15-ZrO_2 samples, both showing a typical sorption behavior observed previously for the alumina supported manganese oxides under similar conditions [11, 21, 22]. The sorption characteristics are also similar for the Mn15-CeO_2 and Mn15-TiO_2 samples, however the measured H_2S concentration profiles depart from the standard behavior as a considerable "pre-breakthrough" concentration is observed. This is a similar feature as observed on the reduced cerium oxide (Fig. 1). As mentioned earlier, one of the reasons for this behavior indicating a slowdown of the gas-solid reaction governing the sorption process may be the diffusion through the increasing sulfidation product layer at the high conversions of the metal oxides. However, the gas-solid reactions are inherently difficult, both from the experimental and data interpretation aspects, thus there might also be some other reasons leading to this behavior.

The development of the sorption capacity over the 13 sorption cycles is presented in Fig. 3. For the sake of the clarity, the maximal capacity is also shown in the figure. This is a theoretical value defined

as the amount of H_2S needed for a complete conversion of MnO to MnS (Reaction 1) considering the actual H_2S flow and the amount of MnO per gram of sample loaded in the reactor.

MnO-support + H_2S ↔ MnS-support + H_2O (1)

The variations in the sorption capacity for the tested materials already indicated in Fig. 2 are further clarified in Fig. 3. The sorption capacity is calculated from the measured H_2S concentration profiles, using the time before reaching the breakthrough, given H_2S flow and the amount of manganese oxide in the sample. Hence, the reported sorption capacities can be regarded as effective sorption capacities rather than the total sorption capacities.

The initial sorption capacity decreases in the following sequence (2):

Mn15-CeO_2 > > Mn15-Al_2O_3 > Mn15-ZrO_2 > Mn15-TiO_2

The highest initial capacity is obtained for the Mn15-CeO_2 sample and the measured capacity exceeds the maximal, theoretical value. The theoretical value is calculated assuming that it is only the manganese oxide that reacts with H_2S (Reaction 1). However, the results presented on CeO_2 show that the cerium oxide itself reacts with H_2S. Therefore there is a certain additive effect when both Mn and Ce oxides capture H_2S. Besides the cerium oxide it was also ZrO_2 that showed a distinct ability to capture H_2S (Fig. 1). In the latter case the additive effect is not apparent as the Mn15-ZrO_2 sample show only moderate sorption capacity comparable to the one observed for the Mn15-Al_2O_3 sample. The different sorption behavior observed for the Ce and Zr oxides upon the functionalization with Mn can be related to the accessibility of the oxygen species for the interaction with sulfur. Both the oxides possess strong basic sites that may interact with the manganese ions contained in the acidic solution of the nitrate precursor during the preparation. During the calcination, residues of the manganese salts and solvating water are removed and some condensation, resulting in bond formation between the support surface oxygen and manganese may occur [23]. This may indicate that the surface lattice oxygen is then less susceptible for the interaction with H_2S and it may rather

be the bulk lattice oxygen that participates in the sorption process. As the additive effect is observed for the Mn15-CeO_2 sample only, it is assumed that the bulk lattice oxygen of the cerium support has more labile character when compared to the Mn15-ZrO_2 sample and can react more readily with H_2S.

When comparing the initial sorption capacity (cycle 1), it is observed that the lowest initial sorption capacity is measured for the Mn15-TiO_2 sample (Fig. 3). The second sorption cycle, and also the 7^{th} and the 12^{th} cycles, were performed after approx.12 h exposure of the sample to H_2 at 650 °C. It was previously observed that this treatment has a significant effect on the performance of the Mn_xO_y-Al_2O_3 sorbents [11]. Here it can be emphasized that the producer gas has a strong reductive character due to the presence of H_2, CO and CH_4. It is therefore essential to know the impact of the reducing environment on the samples performance. Similarly, the sample activation in a reductive gas appears to be relevant to use as it should lead to the species thermodynamically stable in the model producer gas at the given conditions. As seen in Fig. 3, the sorption capacities in the second cycle drop significantly for all the samples when compared to the results from the first sorption cycle. This is a typical behavior observed also by others [22]. It is therefore unlikely that the treatment in H_2 itself that precedes the measurement is responsible for the capacity drop in the second cycle. It is more appropriate to judge the impact of the H_2 pretreatment from the results obtained in cycles 7 and 12. In these cycles, for most of the samples, a substantial drop in the sorption capacity occurs. The only sample that appears to be unaffected by the treatment is the Mn15-ZrO_2 sample. On the other hand, the most pronounced capacity drop is observed for the Mn15-TiO_2 sample. For the latter sample, the sorption capacity was too low. The measured outlet H_2S concentration as high as 1000 ppm was observed already at the beginning of the run, which did not permit the sorption capacity to be calculated in the same manner as for the remaining samples. The Mn_xO_y-Al_2O_3 sorbents tested at 450 °C also showed the lower sorption capacity after the H_2 pre-treatment and similarly as the results presented here, the subsequent exposure to O_2 during the sorbent regeneration recovered the capacity. It was suggested that the H_2 treatment may form species with lesser number of active sites for the interaction with H_2S while the rapid, exothermic O_2 regeneration may recreate the sites [11].

As the capacity drop is most pronounced for the titania-based sample after a high-temperature reduction step another effect, a strong metal-support interaction (SMSI) should be mentioned here as well. In the original paper by Taster et al. introducing the SMSI phenomena a series of experiments was performed on group 8 metals supported on TiO_2 [24]. These experiments, similarly as later on conducted by others [25], included the measurement of the H_2 and CO chemisorption upon various treatments e.g. low, high temperature reduction and oxidation. It was shown that the high temperature reduction remarkably lowers the H_2 and CO uptake which was however nearly completely restored after the oxidative treatment at high temperature (400 °C) [24]. The chemisorption experiments using H_2, CO or O_2 are often used as a measure of the metal dispersion; however the results presented by Taster et al. are quite similar to that what is observed in this work i.e. the drop of the sorption capacity after the high-temperature reduction and its subsequent recovery after the high-temperature oxidative treatment. The SMSI effect is typically observed for titania supported noble metals, however a strong metal-oxide-support interaction as deduced from the XPS measurements was also reported for the titania supported manganese oxides [26]. The SMSI effect leading to the formation of an intermetallic phase between the support and the active specie is associated with supports that are to some extent reducible [24, 25]. Among the examined materials cerium oxide is also reducible and the same effect, a considerable drop in the capacity after the H_2 treatment is also observed when this material is the support. It may suggest that the drop in the capacity can be associated with the SMSI effect in the latter case as well [27]. Interestingly, it is also these two sorbents (Mn15-CeO_2, Mn15-TiO_2) that show the "pre-breakthrough" feature in their sorption characteristic (Fig. 2). As mentioned, the observed sorption behavior is complex and there are likely to be several reasons causing it. However, the SMSI effect might be one of the reasons giving rise to such a behavior. The overall stability of the samples after the H_2 treatment can be represented by the following sequence (3):

Mn15-ZrO_2 > Mn15-CeO_2 ≈ Mn15-Al_2O_3 > Mn15-TiO_2

The data obtained for the Mn15-ZrO_2 sample (Fig. 3, cycle 7 and 12) indicate that the sample sorption performance may actually be slightly improved after the H_2 treatment. Whether the prolonged reduction gives a structure with an enhanced H_2S sorption ability or simply decomposes some remaining sulfidation products by reaction with H_2 at a high temperature and regenerates the sample more thoroughly is impossible to resolve as based on the presented data.

Apart from the partly recoverable sorption capacity drop caused by the H_2 treatment, an overall deactivation of all the samples is observed during the 13 cycles. When comparing the capacities for the first and the last cycle, it is seen in Fig. 3 that the most significant drop is observed for the Mn15-CeO_2 sample while the Mn15-ZrO_2 and Mn15-Al_2O_3 samples show approx. 50 % drop in the capacity values. The least deactivation is observed for the Mn15-TiO_2 sample and its activity in the last cycle is only slightly lower when compared to the other samples. The possible deactivation reasons in detail discussed previously for the Mn_xO_y-Al_2O_3 sorbents included the support transition, transformation of the Mn oxides and incomplete regeneration [11]. In the characterization part, it will be discussed how these aspects may possibly affect the deactivation for the other support than alumina.

Characterization

N_2 sorption measurement

The textural properties of the parent support materials, fresh sorbents as well as the regenerated sorbents as obtained from the N_2 sorption measurements are shown in Table 1. Results collected on the parent supports show a large variation in the sample surface areas ranging from approx. 140 m^2/g obtained for the *γ*-alumina support to approx. 7 m^2/g measured for TiO_2. According to the IUPAC classification, the solids are characterized as mesoporous, having average pore widths in the range 2 – 50 nm. After the functionalization with Mn and subsequent drying and calcination, the surface area becomes lower and there are also some changes in the pore width and volume when

compared to the parent supports. The drop in the surface area was observed previously [11] and is expected as a relative large portion of the porous solid (15 wt. %) is occupied by the Mn oxides that are likely having a low porosity. The changes in the pore width are rather small; however, the pore volume is lowered for most of the samples.

The most pronounced changes in the textural properties are however observed for the samples upon the testing. It appears that the cyclic (sorption/regeneration) operation causes a remarkable drop in the surface area, a noticeable expansion of the pores and a partial loss of the pore volume. This general trend is observed for all the samples except for the pore width assessment of the titania sample. In the previous study, an identical trend was observed for the Mn_xO_y-Al_2O_3 sorbents [11]. It was suggested that the nearly virtual loss of porosity was associated with the alumina transition and sintering. These processes were believed to be induced by the highly exothermic regeneration reaction and the presence of Mn that may possibly accelerate the changes. On the sintering, an agglomeration of the primary sorbent particles takes place which may encapsulate the Mn species responsible for the interaction with H_2S. This may lead to the deactivation as observed in Fig. 3. Similarly, the shrinking surface area of the solids may induce sintering of the manganese oxide, which may result in the formation of particles whose sulfidation/regeneration may become more difficult.

The most significant drop in the sorption capacity is observed for the Mn15-CeO_2 sample (Fig. 3), which is also the sample that shows the largest drop in the surface area after the testing. The structural changes affect strongly the rate of the gas-solid reaction and a rapid sintering will reduce the reaction rate [28]. It can therefore be suggested that the high degree of deactivation observed for the cerium based sample can be caused by its sintering. Provided that the sintering is sufficiently fast and occur to some extent already during the activation, it may also be partially responsible for the "pre-breakthrough" sorption characteristic as observed on the parent CeO_2 sample (Fig. 1). It can be speculated that the sample preparation including calcination at higher temperatures can somehow affect this behavior.

When considering the surface areas of the supported Mn oxides and the initial sorption activity of the corresponding samples (Fig. 3), it is observed that the high surface area of a material will not necessarily mean a high sorption activity. The highest activity is observed for the Mn15-CeO_2 likely due to the additive effect of the Ce and Mn oxides while the surface area is of lesser importance. Similarly, the deactivation rate is not directly proportional to the loss of surface area. In either case the solids textural properties may however give some indication about the sample sorption performance.

X-Ray Diffraction (XRD)

The diffraction patterns obtained for the parent support materials; supported Mn oxides and sorbents regenerated after the 13th cycle are depicted in Fig. 4. As seen in Fig. 4, the crystallographic properties of the parent supports vary significantly and a different degree of crystallinity is observed. The parent *γ*-alumina shows a rather broad diffraction pattern indicating a low degree of the long-range order. The crystallinity degree appears to be higher for ZrO_2 and CeO_2 and even higher for TiO_2 that is characterized by well-defined narrow diffraction lines. The zirconium support consists of monoclinic phase (PDF 00-037-1484) and tetragonal ZrO_2 as indicated by reflection at 2-theta of 30.5° (PDF 01-079-1769). CeO_2 and TiO_2 contain pure cubic fluorite structure (PDF 04-013-4361) and titanium anatase structure (PDF 00-064-0863) respectively.

After the impregnation with Mn and subsequent drying and calcination some new patterns emerge, which is most prominent for the Mn15-Al_2O_3 sample as the new patterns are not superimposed by the support diffraction lines. Upon a closer inspection (Fig. 4), the new features are also observable on the other substrates than alumina. The new diffraction lines observed after the impregnation are attributed to Mn_2O_3. The presence of this oxide can be expected when considering the manganese precursor used, Mn loading and calcination temperature [11, 23, 29, 30]. These factors have a strong influence on the properties of the manganese species formed during the preparation. It was reported

that the use of acetate precursor may lead to the formation of the surface manganese oxide layer on alumina while the use of the nitrate precursor will result in a formation of small crystallinities of manganese oxide on the alumina surface [23]. Herein, the nitrate Mn precursor was used in the sample preparation allowing for a facile one-step impregnation suiting well to a comparative purpose of the study.

The Mn_2O_3 particle size estimated by the Scherrer equation gives comparable particle sizes of 35 and 34 nm for the zirconia and alumina based samples respectively. The Mn_2O_3 particle size on the titania support was slightly higher (approx. 40 nm) while the Mn_2O_3 particle on the CeO_2 support was lower; estimated to be 17 nm. The larger Mn_2O_3 particle size observed for the low surface TiO_2 is somehow expected as the support has a low surface area and thus a limited ability to disperse Mn. Indeed, the monolayer surface coverage estimated to be 0.0532 wt. % Mn per m^2 of the support [31] indicates that a monolayer of Mn oxide is established on all the supports. The largest excess of the Mn species beyond the Mn amount needed for the monolayer formation can then be expected for the low surface titania. This possibly results in the formation of the larger particles. On the other hand, the CeO_2 support may react with the Mn species during the preparation and form solid solution [32] which may restrict the growth of Mn_2O_3 particles. The latter aspect will be also discussed in the Raman section.

Results collected on the regenerated sorbents are also depicted in the Figure 4. Results presented for the Mn15-Al_2O_3-R sample show Mn_3O_4 and $MnAl_2O_4$ phases which is in an agreement with others [21, 22]. The chemistry beyond the spinels formation was discussed in detail previously [11]. It was also suggested that despite the relatively low temperature used for the sorption/regeneration some transition of the *γ*-alumina support can be induced by the presence of Mn and the exothermic regeneration [11]. In this work the exothermic nature of the regeneration was observed when the reactor temperature increased by approx. 15 °C during the regenerations. There was however not a clear trend in the temperature difference measured for the various samples.

For the remaining regenerated sorbents, the presence of the Mn_3O_4 phase is also detected although its diffraction pattern is not that clearly distinguishable from the supports diffraction lines. The obtained patterns also indicate the presence of mixed cerium manganese oxide (PDF 00-064-0204) and $MnTiO_3$ (PDF 00-029-0902) on the CeO_2 and TiO_2 supports respectively. Furthermore, rutile TiO_2 phase (PDF 01-089-0555) is detected on the Mn15-TiO_2-R sample. This indicates that the titania support undergoes a partial phase transformation during the testing. This phase transformation normally occurs at higher temperatures (above 800 °C) [33] which may suggest that the presence of Mn may lower the phase transition temperature as it was proposed for the Mn/alumina system.

The presence of crystalline sulfur species on the regenerated solids may reveal the quality of the regeneration reaction. When conducting the regeneration experiments at 450 °C manganese sulfate was detected by XRD on the regenerated samples [11]. The regeneration performed in this work seems to be more efficient as the XRD patterns do not reveal the presence of sulfates in any of the regenerated sorbents. This is likely to be a result of the higher regeneration temperature used. However, as seen in Fig. 4, the presence of MnS is revealed in the most of the regenerated samples. Furthermore, the presence of cerium-oxide-sulfide Ce_2O_2S (PDF 00-026-1085) is also indicated on the Mn15-CeO_2 sample. This therefore indicates that the complete regeneration of the cerium support and the Mn sorbents is not achieved under the experimental conditions. The only sample that does not clearly show the MnS pattern is the Mn15-TiO_2-R sample. It is difficult to conclude whether this is due to the overlap of the MnS and TiO_2 patterns or due to a more efficient regeneration. It is however observed (Fig. 3) that the latter sample shows the lowest deactivation which may speak in favor of a more complete regeneration.

Raman spectroscopyRaman spectroscopy is a valuable tool to study supported metal oxides. Due to the probing depth it is especially sensitive to the surface species and it is therefore often regarded as a complimentary technique to XRD that gives information about the bulk structure. However, during

the Raman measurements on the Mn oxides, sample fluorescence and instability in the light is often encountered.

The reference Mn oxides and the Mn_xO_y-Al_2O_3 sorbents were studied in detail in the previous works [11, 30]. The most Raman active reference oxide is Mn_3O_4 with a prominent peak at 667 cm^{-1} and additional peaks at 298, 327 and 382 cm^{-1}. Mn_2O_3 and MnO_2 are considerable less Raman active however also these oxides show a characteristic spectral profile. The spectral profile for Mn_2O_3 consists of three main peaks detected at 319, 406, 708 cm^{-1} while MnO_2 shows the Raman peaks at 523, 582 and 656 cm^{-1}. In agreement with others [34], the peaks detected at 667, 705 and 523 cm^{-1} are chosen as the characteristics for Mn_3O_4, Mn_2O_3 and MnO_2 oxides respectively. The exact position of the peaks may vary to some extent due to the samples light sensitivity and the presence of a thin water layer present on the samples when collecting the spectra under ambient conditions [26, 35].

The Raman spectra of the supports used, supported Mn oxides and regenerated sorbents are presented in Fig. 5. The parent γ-alumina does not show any peak in the spectral region used which makes it particularly suitable for the examination of the alumina supported species as long as its fluorescence is suppressed. The spectrum obtained on the Mn15-Al_2O_3 sample is fairly consistent with our previous results reported for the Mn_xO_y-Al_2O_3 sorbents [11]. The peaks detected at approximately 319, 410 and 700 cm^{-1} are associated with the presence of Mn_2O_3, which is expected from the XRD data. Additional features at 520 and a peak shoulder at 660 cm^{-1} are likely related to the presence of MnO_2. The later surface species were not detected by XRD which may suggest that it has an amorphous character. The spectrum recorded on the regenerated sample Mn15-Al_2O_3-R is also in a good agreement with the previous results. The spectrum shows the presence of Mn_3O_4 with its prominent peak at approx. 660 cm^{-1}. Other species detected by XRD on the same sample are not revealed by the Raman measurements.

The spectral profile of ZrO_2 is associated with the presence of the monoclinic and tetragonal ZrO_2 phases, which is in the line with the XRD results. The monoclinic phase (m-ZrO_2) with a prominent

peak at 480 cm^{-1} and the peaks corresponding to the tetragonal phase (t-ZrO2) at 315 and 640 cm^{-1} are clearly recognized in the spectral profile (Fig. 5). The recorded spectrum is in a good agreement with the results reported by others [33, 35]. After the impregnation with Mn, the spectral characteristics of the support nearly disappear and a poorly defined spectrum is obtained (Mn15-ZrO_2). The broad peaks centered at 350, 460, 550 and 640 cm^{-1} are likely to be contributions from both the support as well as the Mn oxides. The spectrum is somehow comparable to that obtained for the Mn15-Al_2O_3 sample although the feature associated with the presence of Mn_2O_3 detected at approx. 700 cm^{-1} for the latter sample is not that well recognized. Instead a broad peak centered at 640 cm^{-1} emerges which may suggest a larger amount of the surface MnO_2. Also the regenerated sample Mn15-ZrO_2-R is comparable to the one recorded on alumina (Mn15-Al_2O_3-R) showing the presence of Mn_3O_4.

The parent TiO_2 support, similarly as reported by others [26, 33, 35], shows the characteristics of the TiO_2 anatase phase with peaks detected at 400, 520 and 640 cm^{-1}. After the functionalization with Mn, the peaks broadening and a peak shoulder at 350 cm^{-1} is observed for the Mn15-TiO_2 sample. The observed changes reflect the presence of the manganese oxide crystals on the TiO_2 surface [26]. For the regenerated sample Mn15-TiO_2-R the anatase spectral characteristics are still preserved, however some new features observed as a broad peak centered at 450 cm^{-1} and a peak shoulder at 620 cm^{-1} are recognized. These features are associated with the rutile TiO_2 phase [33]. A spectral feature at 660 cm^{-1} detected on the Mn15-TiO_2-R sample indicates the presence of Mn_3O_4.

The cerium support exhibits a prominent peak detected at approx. 645 cm^{-1}. This peak is a characteristic of the fluorite structure and is attributed to triply degenerate F_{2g} mode [36]. The spectrum is altered upon the impregnation with Mn as the prominent peak is broadened, shifted towards a lower wavenumber and shows a well-recognized shoulder. Moreover, some broad peaks centered at 560 and 650 cm^{-1} are observed. These observations are consistent with results reported by others for the Ce-Mn systems [32]. Based on the results from Raman and ESR it was suggested

that the perturbation of the fluorite structure was due to formation of solid solution when Mn^{2+} ions substitute Ce^{4+} having a similar radius [32]. The presence of consequently formed oxygen vacancies in the CeO_2 lattice should result in a weak Raman peak at approx. 600 cm^{-1} [36]. This peak is not clearly observed (Fig. 5) due to the presence of Mn oxide and also due to the possible interaction of the Mn oxide with the defect oxygen sites. Interestingly, the prominent peak returns to its original position and becomes sharp indicating improved crystallinity of the sample after the testing (Mn15-CeO_2-R). This may corroborate with the XRD and N_2 sorption results presented earlier indicating sintering of the CeO_2 support. After sintering, a consolidation of the oxide matrix is normally observed which is accompanied by the loss of porosity. It should be re-emphasized that the observed behavior, due to the sampling depth of the Raman laser, represents the surface and subsurface of the solids while the bulk structure can remain relatively unaltered. Besides the changes of the prominent peak shape and position, new features at 325, 375 and 665 cm^{-1} are observed on the regenerated sample (Mn15-CeO_2-R). Similarly as for the remaining regenerated samples, these peaks are likely to be associated with the presence of Mn_3O_4.

Temperature-Programmed Reduction (TPR)

It was mentioned earlier that the producer gas has a reductive character and therefore information regarding the reduction behavior of the tested materials is essential. In a TPR experiment, a solid sample is, on its heating by a specific rate, exposed to a diluted reduction gas e.g. H_2. The gas consumption is measured as a function of temperature and from the measured data; the sample's reduction characteristic is obtained. For more information about the method and information obtainable from the TPR experiments see e.g. [37]. The reduction profiles recorded on the parent supports and fresh sorbents are shown in Fig. 6. As expected for most of the supports nearly no hydrogen uptake is observed. Some minor uptake is however seen for the parent Al_2O_3 and ZrO_2 supports at higher temperatures. These are possible related to water being driven off from the

sample as a consequence of hydroxyl condensation. For the TiO_2 support some minor H_2 uptake is observed as well. In this case some dehydroxylation of the sample occurs as well which is accompanied with the Ti^{4+} to Ti^{3+} reduction. The extent of the titania reduction is minimal, which is to be expected and in agreement with others [26]. However, the titania reduction is one of the reasons for the SMSI effect mentioned earlier. On the other hand, a considerable degree of reduction is observed for the cerium support showing reduction peaks at 540 and 900 °C. The CeO_2 reducibility was a subject of numerous studies and it is generally agreed that the lower temperature peak is associated with the Ce reduction on the surface while the bulk reduction takes place at higher temperatures [38, 39]. Variations in the sample preparation will result in various ratios between the two reduction peaks [39]. This reduction pattern may also be relevant for the sorption behavior of the ceria samples exhibiting the pre-breakthrough H_2S sorption. Several reasons for this behavior were already proposed including the diffusion through the sulfidation product layer and substantial changes in the textural properties. The presented reduction behavior of the ceria support may also suggest that there is some duality of the sorption sites with the first part located on the samples surface and possibly representing the pre-breakthrough and the second part which is less accessible and located in the bulk structure.

The supported Mn oxides (Fig. 6) show some common reduction features. For all the samples except for Mn15-TiO_2, two main reduction peaks are clearly seen and these are accompanied by a rather broad reduction feature detected at lower temperature when compared to the two main peaks. The Mn15-TiO_2 sample shows a shoulder on the main reduction peak with a minor peak at approx. 390 °C. This makes also the reduction behavior of the latter sample comparable with the remaining samples. Beside the three main reduction peaks an additional broad reduction peak is detected at approx. 870 °C for the Mn15-CeO_2 sample. This is most likely related to the reduction of the bulk of CeO_2.

The three step reduction of the supported Mn oxides was observed previously for the Mn_xO_y-Al_2O_3 sorbents [11, 30, 40] and attributed to the reduction of MnO_2 to MnO proceeding through Mn_2O_3 and Mn_3O_4 as indicated in the following sequence (4):

$MnO_2 \rightarrow Mn_2O_3 \rightarrow Mn_3O_4 \rightarrow MnO$

In principle, the main reduction behavior should also be similar for the other supports. Hence, it is proposed that the first peak (Mn15-ZrO_2, Mn15-TiO_2, Mn15-CeO_2) or a broad shoulder (Mn15-Al_2O_3) is due to the reduction of MnO_2 to Mn_2O_3. The presence of surface MnO_2 on Al_2O_3 and ZrO_2 was shown by the Raman spectroscopy. The TPR data suggest that the latter species are to various degrees present on all the samples. The subsequent reduction of Mn_2O_3 to Mn_3O_4 is the second reduction step observed as a reduction peak (Mn15-Al_2O_3, Mn15-ZrO_2, Mn15-CeO_2) or as a shoulder at 495 °C for the Mn15-TiO_2 sample. And finally the Mn_3O_4 reduction to MnO is observed as a strong, high temperature reduction peak that is detected for all the samples.

For the Mn oxides supported on TiO_2 it was proposed that the very first feature observed here as a baseline elevation prior to the first peak at 390 °C can be attributed to the Ti^{4+} to Ti^{3+} reduction because of its interaction with manganese oxide [26]. For the Mn15-CeO_2 sample, reduction of the Mn-Ce solid solution and possibly also some reduction of the surface Ce^{+4} may contribute to the three main reduction peaks.

The fact that the reduction peaks for the various supports are detected at different temperatures suggests a different degree of interactions between the support and Mn. Typically, the higher reduction temperature, the higher degree of the interaction. This would suggest the strongest interaction between Mn and titania, which is not surprising as the strong-metal-support-interaction (SMSI) effect is expected. Mn with alumina is also interacting substantially in this context. In the latter case the effect of the large surface area (largest of all the supports used) giving a large number of anchoring hydroxyl sites is likely responsible for the interaction. The large surface area of the

sample could also cause the broadness of the reduction peaks. This is in contrary to the low surface Mn15-TiO_2 sample showing a poorly resolved reduction pattern.

On the other hand, a considerably weaker interaction may be expected for the Mn15-CeO_2 and Mn15-ZrO_2 as based on the results in Fig. 6. Here a relatively low surface area of the supports certainly plays an important role. Another factor that may be considered in this regard is the reduction behavior of unsupported nano-sized Mn oxides as it was shown that for the Mn oxides the reduction temperature increases with the particle size [41]. This may imply that the sample with the lower Mn particle sizes (Mn15-CeO_2) would be reduced at lower temperature, which agrees with the reported results (Fig. 6).

Conclusion

A series of sorbent materials consisting of manganese oxides supported on various supports was prepared. The presented work then combines the results obtained from the material testing and characterization. As shown, the sorbent performances exhibit noticeable differences in terms the initial sorption capacity, stability during the 13 cycles and stability in H_2. These variations are attributed to the support properties and the way the support interacts with Mn as there was no other variable included neither in the sample preparations nor in the testing. It is shown that the use of a specific supports affects the particle size of the Mn oxide on the calcined solids. The support determines the strength of the Mn oxide/ support interaction and possibly also influences the MnO_2/MnO_3 ratio on the solids after calcination.

An optimal performance with a stable and high H_2S capacity was not observed on any of the tested sorbents as the material with a high initial capacity tend to deactivate rapidly. The deactivation seems to be related not only to the use of the materials at high temperature but also to the reducing atmosphere which the producer gas represents. However, in case of the model producer gas used, it

is shown that the stability in reducing atmosphere is considerably improved when zirconia is used as a support for Mn. The highest initial capacity is observed for cerium supported Mn oxides due to the additive effect. These conclusions may suggest that in a rational design of a new sorbent these two components shall be present in order to achieve the optimal performance.

Acknowledgements

The Norwegian research council is gratefully acknowledged for the financial support through the EnergiX programme; project entitled "Advanced biofuels via synthesis gas" (contract nr. 228741).

References:

[1] W. Torres, S. S. Pansare, J. G. Goodwin, Hot Gas Removal of Tars, Ammonia, and Hydrogen Sulfide from Biomass Gasification Gas, Catalysis Reviews, 49 (2007) 407 – 456

[2] G. W. Huber, S. Iborra, and A. Corma, Synthesis of Transportation Fuels from Biomass: Chemistry, Catalysts, and Engineering, Chemical Reviews, 106 (2006) 4044 – 4098

[3] R. M. Navarro, M. A. Pena, and J. L. G. Fierro, Hydrogen Production Reactions from Carbon Feedstocks: Fossil Fuels and Biomass, Chemical Reviews, 107 (2007) 3952 – 3991

[4] P.L. Spath, D.C. Dayton, Preliminary Screening – Technical and Economic Assessment of Synthesis Gas to Fuels and Chemicals with Emphasis on the Potential for Biomass Derived Syngas, NREL/TP-510-34929 (2003)

[5] D. E. Sparks, G. Jacobs, M. K. Gnanamani, V. R. R. Pendyala, W. Ma, J. Kang, W. D. Shafer, R. A. Keogh, U. M. Graham,P. Gao, B. H. Davis, Poisoning of cobalt catalyst used for Fischer–Tropsch synthesis, Catalysis Today, 215 (2013) 67 – 72

[6] P.V. Aravind, W. de Jong, Evaluation of high temperature gas cleaning options for biomass gasification product gas for Solid Oxide Fuel Cells, Progress in Energy and Combustion Science, 38 (2012) 737 – 764

[7] X. Meng, W. de Jong, R. Pal, A.H.M. Verkooijen, In bed and downstream hot gas desulphurization during solid fuel gasification: A review, Fuel Processing Technology, 91 (2010) 964 – 981

[8] S. Cheah, D.L. Carpenter, K.A. Magrini-Bair, Review of Mid- to High-Temperature Sulfur Sorbents for Desulfurization of Biomass- and Coal-derived Syngas, Energy Fuels, 23 (2009) 5291 – 5307

[9] M. Flytzani-Stephanopoulos, M. Sakbodin, Z. Wang, Regenerative Adsorption and Removal of H_2S from Hot Fuel Gas Streams by Rare Earth Oxides, Science, 312 (2006) 1508 – 1510

[10] P. R. Westmoreland, J. B. Gibson, D. P. Harrison, Comparative Kinetics of High-Temperature Reaction between H_2S and Selected Metal Oxides, Environmental Science & Technology, 11 (1977) 488 – 491

[11] S. Chytil, M. Kure, R. Lødeng, E. A. Blekkan, On the initial deactivation of MnxOy–Al2O3 sorbents for high temperature removal of H2S from producer gas, Fuel Processing Technology 133 (2015) 183–194

[12] J. Kugai, V. Subramani, Ch. Song, M. H. Engelhard, Y.-H. Chin, Effects of nanocrystalline CeO2 supports on the properties and performance of Ni–Rh bimetallic catalyst for oxidative steam reforming of ethanol, J. Catal. 238 (2006) 430 – 440

[13] S. Storsæter, Ø. Borg, E.A. Blekkan, A. Holmen, Study of the effect of water on Fischer–Tropsch synthesis over supported cobalt catalysts, J. Catal. 231 (2005) 405 – 419

[14] J.C.P. Broekhoff, J.H. De Boer, Studies on Pore Systems in Catalysts: IX calculation of pore distribution from the adsorption branch of nitrogen sorption isotherms in the case of open cylindrical pores A. Fundamental equations, J. Catal. 9 (1967) 8

[15] Ø. Borg, S. Eri, E.A. Blekkan, S. Storsæter, H. Wigum, E. Rytter, A. Holmen, Fischer–Tropsch synthesis over γ-alumina-supported cobalt catalysts: Effect of support variables, J. Catal., 248 (2007) 89 – 100

[16] Y. Zeng, S. Zhang, F.R. Groves, D.P. Harrison, High temperature gas desulfurization with elemental sulfur production, Chemical Engineering Science 54 (1999) 3007 – 3017

[17] Y. Zeng, S. Kaytakoglu, D. P. Harrison, Reduced cerium oxide as an efficient and durable high temperature desulfurization sorbent, Chemical Engineering Science 55 (2000) 4893 – 4900

[18] M. Ziolek, J. Kujawa, O. Saur, J.C. Lavalley, Influence of hydrogen sulfide adsorption on the catalytic properties of metal oxides, Journal of Molecular Catalysis A: Chemical 97 (1995) 49 – 55

[19] M. Ziolek, J. Kujawa, O. Saur, J.C. Lavalley, Metal Oxides as Catalysts for the Reaction between Methanol and Hydrogen Sulfide, J. Phys. Chem., 97 (1993) 9761 – 9766

[20] E.I. Kauppi, J.M. Kanervo, J. Lehtonen, L. Lefferts, Interaction of H_2S with $ZrO_2$and its influence on reactivity of surface oxygen, Appl. Catal. B: Environ. 164 (2015) 360–370

[21] W.J.W. Bakker, F. Kapteijn, J.A. Moulijn, A high capacity manganese-based sorbent for regenerative high temperature desulfurization with direct sulfur production, Chemical Engineering Journal, 96 (2003) 223 – 235

[22] J.P. Wakker, A.W. Gerritsen, J.A. Moulijn, High Temperature H_2S and COS Removal with MnO and FeO on γ-Al_2O_3, Ind. Eng. Chem. Res., 32 (1993) 139 – 149

[23] F. Kapteijn, A.D. v Langeveld, J.A. Moulijn, A. Anreini, M.A. Vuurman, A.M. Turek, J.M. Jehng, I.E. Wachs, Alumina-Supported Manganese Oxide Catalysts: I. Characterization: Effect of Precursor and Loading, J. Catal., 150 (1994) 94 – 104

[24] S. J. Tauster, S. C. Fung, R. L. Garten, Strong Metal-Support Interactions. Group 8 Noble Metals Supported on TiO_2, Journal of the American Chemical Society, 100 (1978) 170 – 175

[25] A. D. Logan, E. J. Braunschweig, A. K. Datye, D. J. Smith, Direct observation of the surfaces of small metal crystallites: rhodium supported on titania, Langmuir, 4 (1988) 827

[26] P.R. Ettireddy, N. Ettireddy, S. Mamedov, P. Boolchand, P.G. Smirniotis, Surface characterization studies of TiO_2 supported manganese oxide catalysts for low temperature SCR of NO with NH_3, Appl. Catal. B: Environ., 76 (2007) 123 – 134

[27] Y. Lin, Z. Wu, J. Wen, K. Ding, X. Yang, K. R. Poeppelmeier, L. D. Marks, Adhesion and Atomic Structures of Gold on Ceria Nanostructures: The Role of Surface Structure and Oxidation State of Ceria Supports, Nano Lett. 15 (2015) 5375−5381

[28] J. Szekely, J.W. Evans, H.Y. Sohn, Gas–Solid reactions, Academic Press, New York (1976), p. 101

[29] B.R. Strohmeier, D.M. Hercules, Surface Spectroscopic Characterization of Mn/Al_2O_3 catalysts, J. Phys. Chem., 88 (1984) 4922 – 4929

[30] S. Chytil, A. Lind, E. Vanhaecke, E. A. Blekkan, Preparation and Characterization of Mn_xO_y-Al_2O_3 Sorbents for H_2S Removal from Biomass Gasification Gas, Energy Procedia, 26 (2012) 98 – 106

[31] J. M. Gallardo-Amores, T. Armaroli, G. Ramis, E. Finocchio, G. Busca, A study of anatase–supported Mn oxide as catalysts for 2-propanol oxidation, Appl. Catal. B: Environ. 22 (1999) 249 – 259

[32] W.-J. Hong, S. Iwamoto, S. Hosokawa, K. Wada, H. Kanai , M. Inoue, Effect of Mn content on physical properties of CeO_x–MnO_y support and BaO–CeO_x–MnO_y catalysts for direct NO decomposition, J. Catal. 277 (2011) 208 – 216

[33] I. Atribak, I. S. Basáñez, A. B.López, A. G. García Comparison of the catalytic activity of MO_2 (M = Ti, Zr, Ce) for soot oxidation under NO_x/O_2, J. Catal. 250 (2007) 75 – 84

[34] F. Buciuman, F. Patcas, R. Craciun, D.R.T. Zahn, Vibrational spectroscopy of bulk and supported manganese oxides, Phys. Chem. Chem. Phys., 1 (1999) 185 – 190

[35] I. E. Wachs, Raman and IR studies of surface metal oxide species on oxide supports: Supported metal oxide catalysts, Catalysis Today, 27 (1996) 437 – 455

[36] B. M. Reddy, K. N. Rao, G. K. Reddy, A. Khan, S.-E. Park, Structural Characterization and Oxidehydrogenation Activity of CeO_2/Al_2O_3 and $V_2O_5/CeO_2/Al_2O_3$ Catalysts, J. Phys. Chem. C 111 (2007) 18751 – 18758

[37] H. Knozinger, Temperature-Programmed Reduction and Oxidation, in: H. Knozinger, G. Erlt, J. Weitkamp (eds.), Handbook of Heterogeneous Catalysis, Wiley-WCH (2008) 1080 – 1096

[38] C. Bigey, L. Hilaire, G. Maire, WO_3–CeO_2 and Pd/WO_3–CeO_2 as Potential Catalysts for Reforming Applications, J. Catal. 198 (2001) 208 – 222

[39] F. Giordano, A. Trovarelli, C. de Leitenburg, M. Giona, A Model for the Temperature-Programmed Reduction of Low and High Surface Area Ceria, J. Catal. 193 (2000) 273 – 282

[40] F. Kapteijn, L. Singoredjo, A. Anreini, J.A. Moulijn, Activity and selectivity of pure manganese oxides in the selective catalytic reduction of nitric oxide with ammonia, Appl. Catal. B: Environ., 3 (1994) 173 – 189

[41] J. Pike, J. Hanson, L. Zhang, S.-W. Chan, Synthesis and Redox Behavior of Nanocrystalline Hausmannite (Mn_3O_4), Chem. Mater., 19 (2007**)** 5609 – 5616

Figures and tables

Figure 1.

H_2S concentration profiles (H_2S in the exit gas as a function of time) measured over H_2 treated metal oxides at 650 °C and 101.325 kPa. Feed gas composition 0.4, 39.6, 40.0 and 20 vol. % for H_2S, Ar, H_2 and N_2 respectively. For the sake of the clarity, the concentration profiles are normalized to 0.4 vol. % (4000 ppm) H_2S reactor inlet concentration and shifted along the y-axis.

Figure 2.

H_2S concentration profiles (H_2S in the exit gas as a function of time) measured over reduced Mn supported oxide at 650 °C and 101.325 kPa. Feed gas composition was 0.4, 39.6, 40.0 and 20 vol. % for H_2S, Ar, H_2 and N_2 respectively. For the sake of the clarity, the concentration profiles are normalized to 0.4 vol. % (4000 ppm) H_2S reactor inlet concentration and shifted along the y-axis. Data collected on the support materials depicted by dashed lines.

Figure 3.

Sorbent capacity development measured over 13 sorption/regeneration cycles. Cycles 2, 7 and 12 are performed after approx. 12 h exposure to H_2/N_2 at 650 °C.

Figure 4.

XRD patterns for parent supports, fresh Mn sorbents and sorbents regenerated after the 13th sorption cycle. • Mn_2O_3 (PDF 00-041-1442), ° Mn_3O_4 (PDF 04-007-1841), * MnS (PDF 00-040-1289), □ $MnAl_2O_4$ (PDF 00-029-0880)

Figure 5.

Vis-Raman spectra of parent supports, fresh Mn sorbents and sorbents regenerated after the 13th sorption cycle.

Figure 6.

TPR profiles recorded on parent supports and fresh Mn sorbents.

Table 1.

Textural properties of parent supports, fresh Mn sorbents and regenerated sorbents upon multiple sorption/regeneration cycles

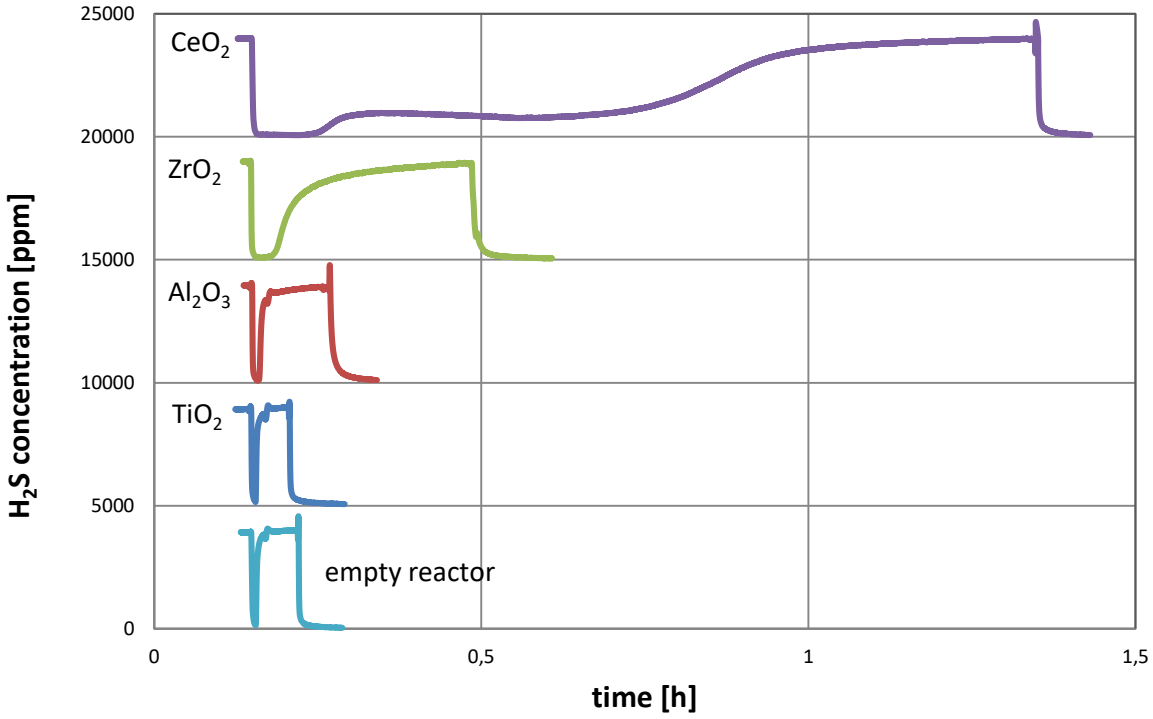
25000
20000
15000
10000
5000
0
CeO2
ZrO2
Al2O3
TiO2
empty reactor
0
0,5
1
1,5
H2S concentration [ppm]
time [h]

Figure 1.

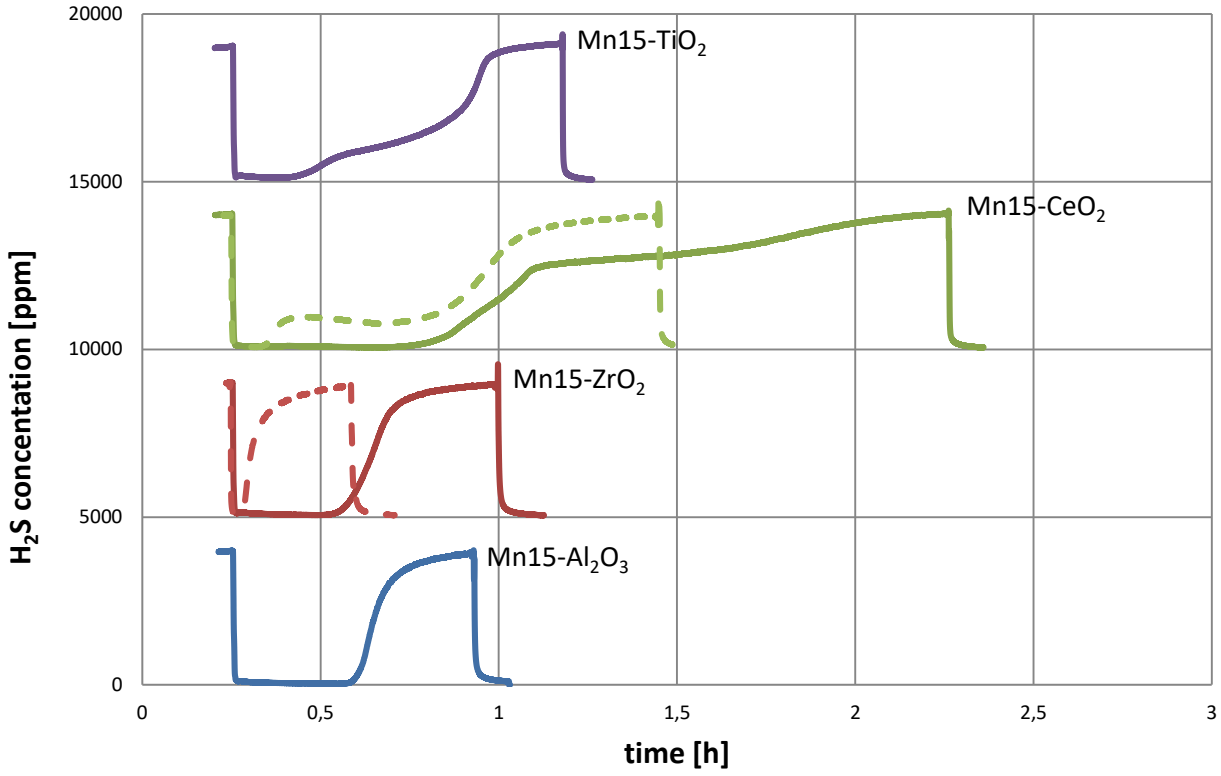
20000
15000
10000
5000
0
H2S concentation [ppm]
0
0,5
1
1,5
2
2,5
3
time [h]
Mn15-TiO2
Mn15-CeO2
Mn15-ZrO2
Mn15-Al2O3

Figure 2.

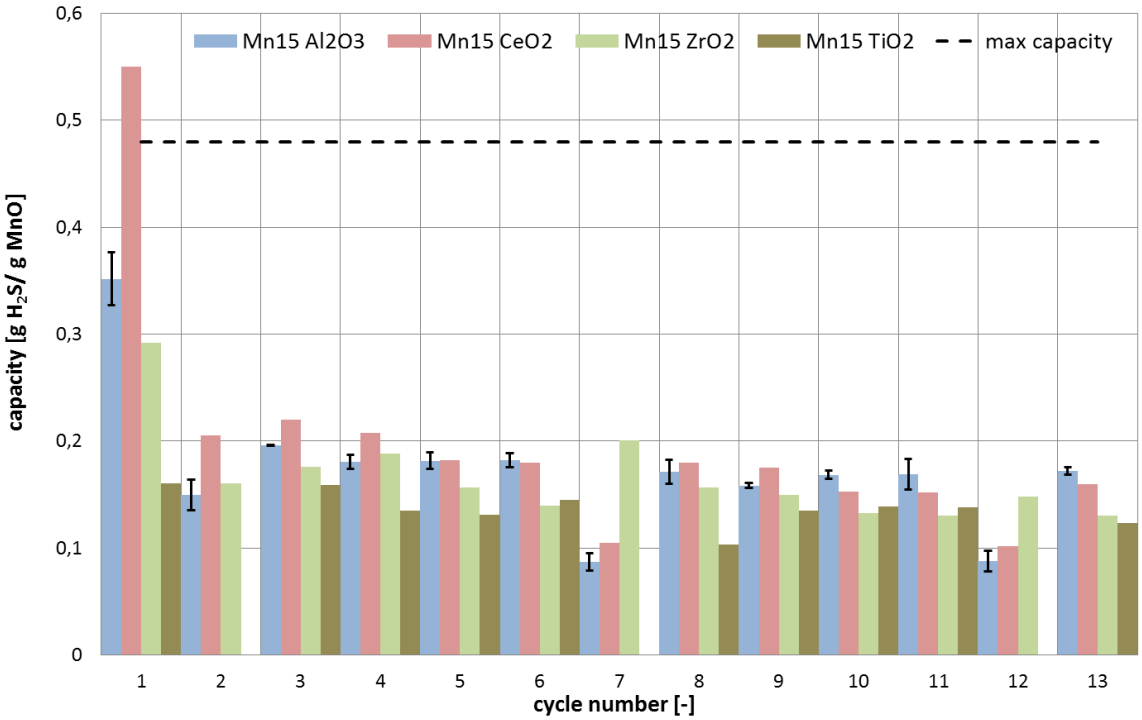
Mn15 Al2O3
Mn15 CeO2
Mn15 ZrO2
Mn15 TiO2
max capacity
capacity [g H2S/ g MnO]
0,6
0,5
0,4
0,3
0,2
0,1
0
1
2
3
4
5
6
7
8
9
10
11
12
13
cycle number [-]

Figure 3.

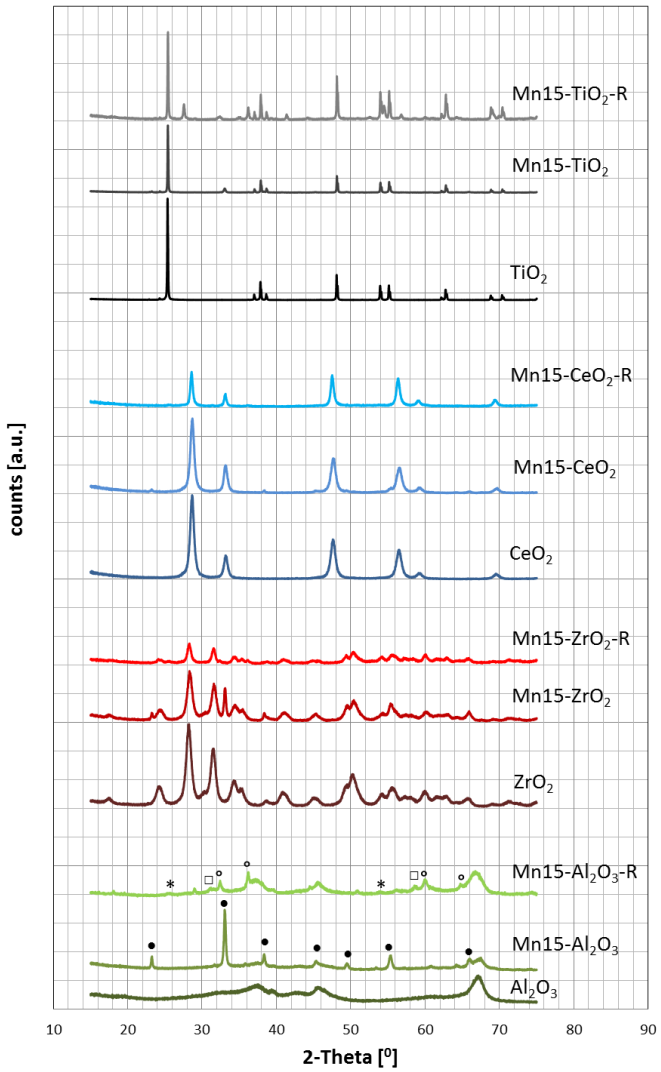
Mn15-TiO2-R
Mn15-TiO2
TiO2
Mn15-CeO2-R
Mn15-CeO2
CeO2
Mn15-ZrO2-R
Mn15-ZrO2
ZrO2
Mn15-Al2O3-R
Mn15-Al2O3
Al2O3
counts [a.u.]
10
20
30
40
50
60
70
80
90
2-Theta [⁰]

Figure 4.

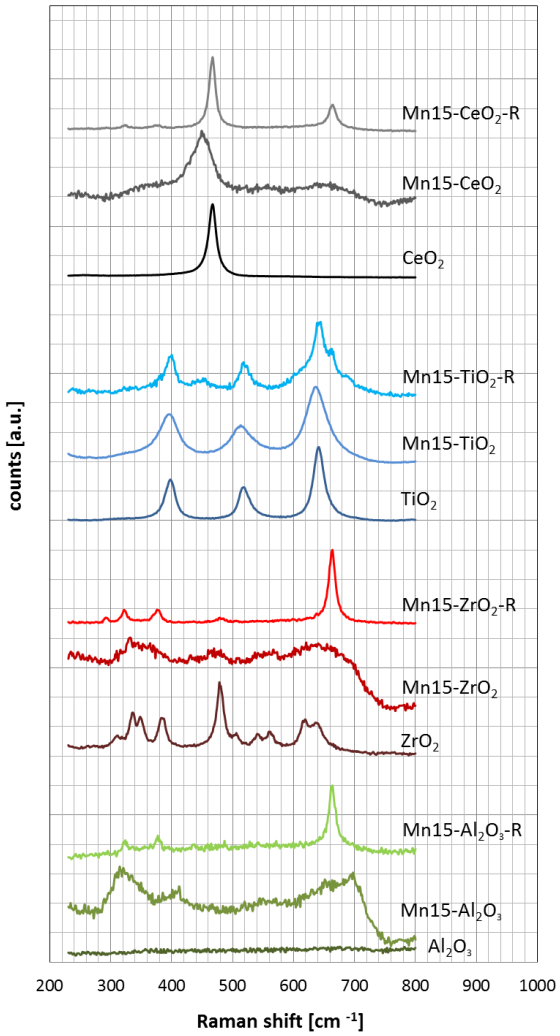
Mn15-CeO2-R
Mn15-CeO2
CeO2
Mn15-TiO2-R
Mn15-TiO2
TiO2
Mn15-ZrO2-R
Mn15-ZrO2
ZrO2
Mn15-Al2O3-R
Mn15-Al2O3
Al2O3
counts [a.u.]
200
300
400
500
600
700
800
900
1000
Raman shift [cm -1]

Figure 5.

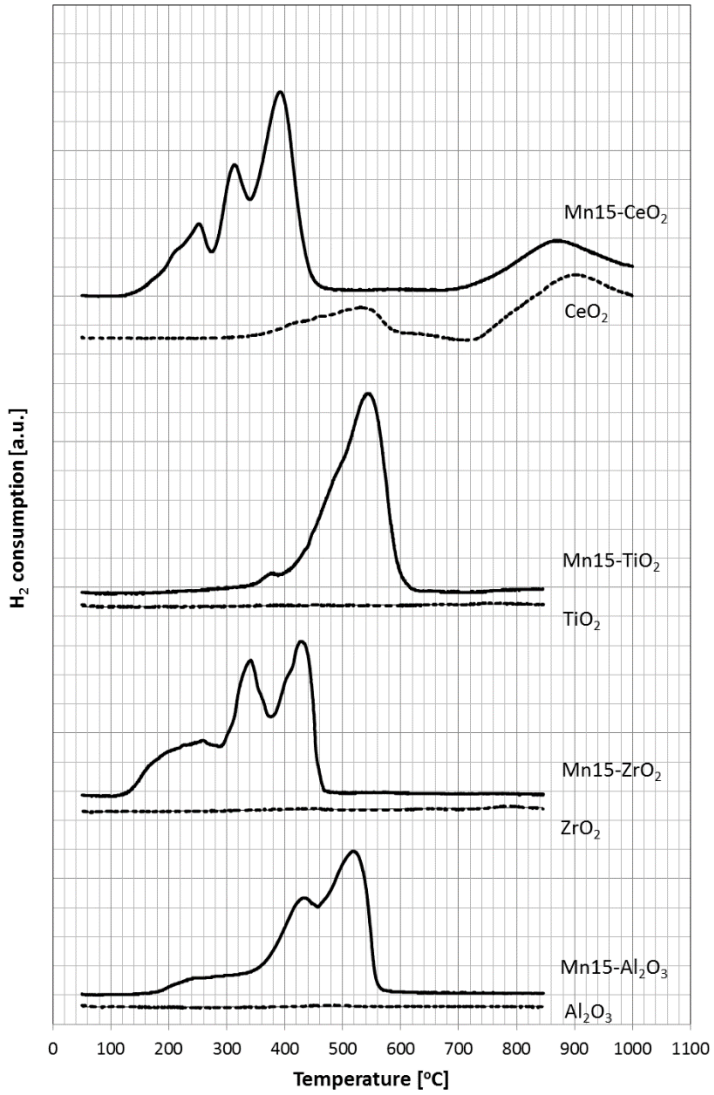
Mn15-CeO2
CeO2
Mn15-TiO2
TiO2
Mn15-ZrO2
ZrO2
Mn15-Al2O3
Al2O3
H2 consumption [a.u.]
0
100
200
300
400
500
600
700
800
900
1000
1100
Temperature [°C]

Figure 6.

Sample	Surface area [m^2/g]	Pore width[a] [nm]	Pore volume[b] [cm^3/ g]
Al_2O_3	139.8	5.5	0.2715
Mn-Al_2O_3	104.5	5.7	0.2010
Mn-Al_2O_3-R	61.2	8.1	0.1761
ZrO_2	77.5	10.1	0.2834
Mn-ZrO_2	63.0	9.9	0.2145
Mn-ZrO_2-R	18.2	20.6	0.1448
CeO_2	48.2	17.6	0.1719
Mn-CeO_2	33.1	16.9	0.1288
Mn-CeO_2-R	2.7	50.5	0.0400
TiO_2	7.4	2.6	0.0358
Mn-TiO_2	6.7	30.6	0.0445
Mn-TiO_2-R	4.7	2.6	0.0234

[a] – from Broekhoff-de Boer algorithm applied on the adsorption branch of N_2 isotherm

[b] – accumulated pore volume